

Stephen F. Austin State University SFA ScholarWorks

Faculty Publications

Biology

2007

Full-Length, Glycosylated NSP4 is Localized to Plasma Membrane Caveolae by a Novel Raft Isolation Technique

Stephen M. Storey

Texas A & M University - College Station

Thomas F. Gibbons

Texas A & M University - College Station

Cecelia V. Williams

Texas A & M University - College Station

Rebecca D. Parr


Stephen F Austin State University, parrrl@sfasu.edu

Friedhelm Schroeder

Texas A & M University - College Station

See next page for additional authors

Follow this and additional works at: <http://scholarworks.sfasu.edu/biology>

 Part of the [Biology Commons](#), and the [Biotechnology Commons](#)

Tell us how this article helped you.

Recommended Citation

Storey, Stephen M.; Gibbons, Thomas F.; Williams, Cecelia V.; Parr, Rebecca D.; Schroeder, Friedhelm; and Ball, Judith M., "Full-Length, Glycosylated NSP4 is Localized to Plasma Membrane Caveolae by a Novel Raft Isolation Technique" (2007). *Faculty Publications*. Paper 47.

<http://scholarworks.sfasu.edu/biology/47>

This Article is brought to you for free and open access by the Biology at SFA ScholarWorks. It has been accepted for inclusion in Faculty Publications by an authorized administrator of SFA ScholarWorks. For more information, please contact cdsscholarworks@sfasu.edu.

Authors

Stephen M. Storey, Thomas F. Gibbons, Cecelia V. Williams, Rebecca D. Parr, Friedhelm Schroeder, and
Judith M. Ball

Full-Length, Glycosylated NSP4 Is Localized to Plasma Membrane Caveolae by a Novel Raft Isolation Technique[∇]

Stephen M. Storey,¹ Thomas F. Gibbons,¹ Cecelia V. Williams,¹ Rebecca D. Parr,¹
Friedhelm Schroeder,² and Judith M. Ball^{1*}

Department of Pathobiology, Texas Veterinary Medical Center, Texas A&M University, TAMU 4467, College Station, Texas 77843-4467,¹ and Department of Physiology and Pharmacology, Texas A&M University, TAMU 4466, College Station, Texas 77843-4466²

Received 25 August 2006/Accepted 16 March 2007

Rotavirus NSP4, initially characterized as an endoplasmic reticulum intracellular receptor, is a multifunctional viral enterotoxin that induces diarrhea in murine pups. There have been recent reports of the secretion of a cleaved NSP4 fragment (residues 112 to 175) and of the association of NSP4 with LC3-positive autophagosomes, raft membranes, and microtubules. To determine if NSP4 traffics to a specific subset of rafts at the plasma membrane, we isolated caveolae from plasma membrane-enriched material that yielded caveola membranes free of endoplasmic reticulum and nonraft plasma membrane markers. Analyses of the newly isolated caveolae from rotavirus-infected MDCK cells revealed full-length, high-mannose glycosylated NSP4. The lack of Golgi network-specific processing of the caveolar NSP4 glycans supports studies showing that NSP4 bypasses the Golgi apparatus. Confocal imaging showed the colocalization of NSP4 with caveolin-1 early and late in infection, elucidating the temporal and spatial NSP4-caveolin-1 association during infection. These data were extended with fluorescent resonance energy transfer analyses that confirmed the NSP4 and caveolin-1 interaction in that the specific fluorescently tagged antibodies were within 10 nm of each other during infection. Cells transfected with NSP4 showed patterns of staining and colocalization with caveolin-1 similar to those of infected cells. This study presents an endoplasmic reticulum contaminant-free caveola isolation protocol; describes the presence of full-length, endoglycosidase H-sensitive NSP4 in plasma membrane caveolae; provides confirmation of the NSP4-caveolin interaction in the presence and absence of other viral proteins; and provides a final plasma membrane destination for Golgi network-bypassing NSP4 transport.

Rotaviruses (RV) are the leading viral etiologic agents of severe pediatric gastroenteritis worldwide, affecting nearly all children before the age of 5, with 2 million cases resulting in 444,000 deaths annually (33, 34, 40). RV nonstructural protein 4 (NSP4) was initially characterized as an endoplasmic reticulum (ER) transmembrane glycoprotein due to the protein's high-mannose glycosylation and its critical function as an intracellular receptor for the translocation of subviral particles into the ER during virion morphogenesis (2, 5, 14). However, the identification of NSP4 and NSP4 amino acids (aa) 114 to 135 (NSP4₁₁₄₋₁₃₅) as enterotoxic and the redistribution of RV-encoded proteins upon NSP4 silencing led to a reevaluation of NSP4 function(s) and subcellular localization(s) (4, 31).

A cleaved NSP4 fragment, aa 112 to 175, is secreted from RV-infected epithelial cells, indicating that some portion of NSP4 traffics from the ER to the plasma membrane (PM) (65). The colocalization of NSP4₁₁₄₋₁₃₅ and the extracellular matrix proteins laminin-β3 and fibronectin at the basement membrane of small-intestinal epithelia from RV strain EDIM-infected mouse pups also supports NSP4 transport to the PM during host infection (8). While both findings demonstrate that at least a fragment of NSP4 leaves the ER of infected cells,

neither confirms the presence of full-length NSP4 at the PM nor reveals the specific distribution of the viral glycoprotein in PM lipid microdomains. The detection of NSP4 in Triton X-100-resistant lipid rafts isolated from RV-infected Caco-2 cells indicates that the viral enterotoxin may be a resident of cellular lipid rafts during infection (11, 49).

The biophysical structures and compositions of cellular lipid rafts remain controversial, as lipid rafts are defined primarily operationally as a collection of cellular membranes insoluble in nonionic detergents at 4°C. These detergent-resistant membranes (DRM) have a unique lipid composition, enriched with cholesterol, sphingomyelin, and glycolipids, producing a liquid-ordered or gel-phase raft with a low density that is buoyant on sucrose gradients (15, 55). Ganglioside M1 (G_{M1}), glycerophosphatidylinositol-anchored proteins, flotillin, and caveolins have been used as markers for measuring the enrichment of DRM following isolation from cell lysates or membrane fractions (53, 54). Yet the ability of detergents to both cluster and remove cellular membrane proteins and lipids illustrates that DRM do not represent the actual composition of all rafts in the cell (19, 57).

Caveolae are a subset of lipid rafts defined by the presence of caveolin proteins (caveolin-1, -2, or -3) (50, 51). Despite the recent use of detergent-free isolation, caveola composition is nearly as controversial as that of rafts due to the confusing and often conflicting data resulting from the use of different cell types and isolation procedures (44). Using a sodium carbonate homogenization buffer with a high pH and sucrose gradients to isolate caveolae from myocytes yields a caveolin-3-enriched

* Corresponding author. Mailing address: Department of Pathobiology, TVMC, Texas A&M University, TAMU 4467, College Station, TX 77843-4467. Phone: (979) 845-7910. Fax: (979) 845-9231. E-mail: jball@cvm.tamu.edu.

[∇] Published ahead of print on 21 March 2007.

fraction without detectable clathrin, Na/K-ATPase (a nonraft PM marker), and mannosidase II (a Golgi apparatus marker) (64), whereas the same protocol with PM-enriched material from another cell type yields a caveolin-1-enriched fraction that contains both clathrin and Na/K-ATPase (18). Other caveola isolation protocols, such as anticaveolin affinity chromatography and density gradient fractionation of caveolae sheared from silica-coated PM, successfully extract caveolin-containing membranes, but these fractions have yet to be assayed for similar ranges of organelle- and vesicle-specific markers (53, 56, 58).

We have reported that NSP4 may specifically partition into caveolae during infection. NSP4 and NSP4₁₁₄₋₁₃₅ preferentially interact with highly curved model membranes enriched with cholesterol and anionic phospholipids (20, 21). Specific secondary structure alterations (increased helical content) upon interaction with different model membranes demonstrate that NSP4 and NSP4₁₁₄₋₁₃₅ associate with membranes that mimic caveolae (20). Although this study utilizes model membranes lacking proteins, we also show the colocalization of NSP4 with caveolin-1 both at intracellular sites and at the peripheries of RV-infected MDCK and Caco-2 cells, as well as a direct interaction between NSP4 and caveolin-1, by yeast two-hybrid, *in vitro* binding, and coimmunoprecipitation assays (41). Based on these data, we hypothesize that full-length NSP4 traffics from the ER to PM caveolae during RV infection of epithelial cells. To examine this hypothesis, we generated a detergent-free isolation method optimized to produce a PM caveola-enriched fraction from epithelial cells that contained caveola markers and were devoid of detectable Golgi apparatus, ER, clathrin-coated pit, and liquid-phase (nonraft) PM markers. An analysis of the PM caveolae isolated in this manner from RV-infected cells revealed that full-length NSP4 was present and was doubly glycosylated with high-mannose-content glycans.

MATERIALS AND METHODS

Antibodies and reagents. Antibodies directed against Na/K-ATPase α (mouse anti-sheep Na/K-ATPase α ; Affinity BioReagents, Inc., Golden, CO), calnexin (rabbit anti-canine calnexin aa 575 to 593; Stressgen Biotech, Victoria, BC, Canada), golgin-97 (mouse anti-human golgin-97; Molecular Probes, Eugene, OR), giantin (rabbit anti-human giantin aa 1 to 469; Covance Research Products, Inc., Princeton, NJ), flotillin-1 (mouse anti-mouse flotillin-1 aa 312 to 428), caveolin-1 (rabbit anti-caveolin-1 aa 68 to 75), clathrin (mouse anti-rat clathrin heavy chain aa 4 to 171; BD Transduction Lab, Lexington, KY), and cholera toxin (rabbit anti-*Vibrio cholerae* toxin; Sigma-Aldrich, St. Louis, MO) were purchased from the indicated commercial sources. Horseradish peroxidase-conjugated goat anti-rabbit and anti-mouse immunoglobulin G (IgG; Southern Biotech Association, Inc., Birmingham, AL) and alkaline phosphatase-conjugated goat anti-rabbit IgG (Sigma-Aldrich) were purchased commercially. Linked antibodies and fluorescent molecules included goat anti-mouse IgG-Texas Red (Rockland Immunochemicals, Inc., Gilbertville, PA), the F(ab')₂ fragment of goat anti-mouse and anti-rabbit antibody-Cy2 (Jackson ImmunoResearch), and goat anti-rabbit IgG-fluorescein isothiocyanate (IgG-FITC; KPL, Inc., Gaithersburg, MD). Antibodies specific to the NSP4 peptide aa 150 to 175 (NSP4₁₅₀₋₁₇₅; deduced from the simian rotavirus SA11 NSP4 sequence) were generated in rabbits and mice by using peptide cross-linked to keyhole limpet hemocyanin as an antigen (41).

Purified cholera toxin B subunit (CT-B; Sigma-Aldrich), 5-bromo-4-chloro-3'-indolylphosphate *p*-toluidine (BCIP)-nitroblue tetrazolium chloride premixed electrophoresis reagent (Sigma-Aldrich), concanavalin A (ConA)-Sepharose 4B (Amersham Pharmacia Biotech, Piscataway, NJ), α -methyl-D-mannopyranoside (Acros Organics/Fisher Scientific International, Inc., Hampton, NH), endo- β -N-acetylglucosaminidase H (endo H; New England BioLabs, Ipswich, MA), pro-

tease inhibitor cocktail set III (Calbiochem, Darmstadt, Germany), and 0.45- μ m-pore-size pure nitrocellulose filters (GE Osmonics Labstore, Minnetonka, MN) were acquired from the indicated commercial sources.

Generation of anti-NSP4₁₅₀₋₁₇₅ Fab segments. NSP4₁₅₀₋₁₇₅-specific antibodies were affinity purified before use in confocal microscopy, and Fab fragments were generated for fluorescent resonance energy transfer (FRET) analyses to reduce the distances of the fluorophores from the target proteins. Rabbit anti-NSP4₁₅₀₋₁₇₅ was affinity purified on an NSP4₁₅₀₋₁₇₅ peptide column prepared with preactivated cyanogen bromide Sepharose 4B beads by following the instructions of the manufacturer (Pharmacia Biotech) (3). The bound peptide IgG was eluted by altering the pH (60). The ImmunoPure F(ab)₂ preparation kit (Pierce, Rockford, IL) was utilized, and the recommended protocol was followed with the exception that immobilized papain was substituted for immobilized pepsin to produce Fab versus F(ab)₂ (62). Cy3 monofunctional reactive dye was conjugated to the affinity-purified NSP4₁₅₀₋₁₇₅ Fab fragment for FRET analyses exactly as described by the manufacturer (Amersham Bioscience).

Cultured cells and virus. MDCK (American Type Culture Collection, Manassas, VA) and HT29.f8 cells, a spontaneously polarizing cell line derived from the human adenocarcinoma HT29 intestinal cell line (36), were grown in maintenance medium (Dulbecco's modified Eagle's medium [DMEM] with 4.5 g/liter glucose, L-glutamine, and sodium pyruvate; Mediatech, Inc., Herndon, VA) supplemented with 2 mM L-glutamine (BioWhittaker/Cambrex), 1 mM sodium pyruvate (Cambrex), 0.1 mM nonessential amino acids (Mediatech, Inc.), 100 U/liter penicillin, 100 μ g/liter streptomycin, 0.25 μ g/liter amphotericin B (10,000 U of penicillin–10,000 U of streptomycin–25 μ g/liter amphotericin B; Cambrex), 43.9 mM sodium bicarbonate (GIBCO), 5% fetal bovine serum, and 5% Serum Supreme (Cambrex) at 37°C in 5% CO₂. MDCK cell stocks were maintained in 175-cm² flasks and expanded into 500-cm² trays or 2-cm² multiwell plates (Corning, Inc., Corning, NY) for caveola isolation. MDCK cells were infected with RV SA11 clone 4F (gift of Mary Estes, Baylor College of Medicine, Houston, TX) at a multiplicity of infection (MOI) of 2 PFU/cell. Briefly, the virus was sonicated (5 min with an ice bath in the cuphorn attachment of a Sonicator 3000; Misonix, Inc., Farmingdale, NY), incubated in serum-free DMEM with 5 μ g/ml trypsin for 30 min at 37°C, and then incubated with the cells for 60 min at 37°C in 5% CO₂. The inoculum was replaced with serum-free DMEM supplemented with 1 μ g/ml trypsin, and the cells were incubated for an additional 7.5 or 24 h. The HT29.f8 cells were grown on glass coverslips for confocal imaging and FRET analyses. Prior to infection, all cells were starved for fetal bovine serum for 10 to 16 h. RV SA11 4F was treated with trypsin at a concentration of 10 μ g/ml for 30 min and then applied to cells for 1 h at an MOI of 2 PFU/cell.

NSP4 transfection. MDCK and HT29.f8 cells were transiently transfected with pcDNA3.2D NSP4₁₋₁₇₅ plasmid DNA by using nucleofection, a delivery system in which DNA is delivered directly into the nuclei of the cells. The Nucleofector II device and Nucleofector I kits were used according to the protocols designed by Amaxa Biosystems (Cologne, Germany). Briefly, the cells were grown to 60 to 70% confluence ($\sim 3.5 \times 10^5$ cells/cm² for MDCK cells and $\sim 5.5 \times 10^5$ cells/cm² for HT29.f8 cells), and the appropriate numbers of cells (5×10^5 MDCK cells and 1×10^6 HT29.f8 cells) were harvested, mixed with the cell type-specific Nucleofector solution and NSP4₁₋₁₇₅ plasmid DNA, subjected to nucleofection (using Nucleofector programs A-024 and W-017 for MDCK cells and HT29.f8 cells, respectively), plated onto 10-mm coverslips, and incubated for 20 h. After the removal of the growth medium and washing with phosphate-buffered saline (PBS), the transfected cells were fixed and permeabilized with ice-cold methanol-acetone (1:1).

DRM isolation. DRM were isolated from MDCK cells as previously described (49). Briefly, four 500-cm² trays of cells were grown to confluence ($\sim 6 \times 10^7$ cells/tray), washed with PBS, and scraped into a 4-ml final volume of TNE buffer (20 mM Tris-HCl [pH 7.4], 150 mM NaCl, 1 mM EDTA, 0.2 μ M phenylmethylsulfonyl fluoride [PMSF], and 1% Triton X-100). The suspended cells were passed 10 times through a 22-gauge needle, and the homogenate was incubated for 30 min at 4°C before mixing with 2.5 M sucrose to a density of 40%. A 40%-35%-5% discontinuous sucrose density gradient was centrifuged at 180,000 $\times g$ at 4°C for 18 h (by using a Beckman SW41Ti rotor and an Optima LE-80k ultracentrifuge), and the DRM were recovered from the 35%-5% interface. For Western blot analyses, the DRM and detergent-soluble membrane (DSM) proteins (40% gradient layer) were further processed by ultracentrifugation (190,000 $\times g$ for 1.5 h with a Beckman SW41Ti rotor) in Tris buffer (10 mM Tris, 1 mM EDTA) and suspended in PBS for protein quantification or in PBS containing 0.2 μ M PMSF and 1 μ l/ml protease inhibitor cocktail set III for cold storage at -80°C . All membrane isolations were completed on ice unless otherwise noted.

Cavitation-sucrose chromatography (CSC) caveola isolation. PM-derived caveolae were isolated by using a sucrose density gradient and ConA affinity chromatography as described previously (15). Briefly, MDCK cells were grown in

four to eight trays (500 cm²), washed twice with PBS, and scraped into an 8-ml final volume. Cells were pelleted for 5 min at 1,000 × *g* at room temperature (RT), suspended in a 2-ml solution of 0.25 M sucrose, 1 mM EDTA, and 20 mM Tris base, pH 7.8, and homogenized by nitrogen gas cavitation (15 min at 40 lb/in²) (1, 27). The nuclei and remaining intact cells were pelleted by centrifugation for 10 min at 1,000 × *g* at RT. The original cell supernatant and post-nuclear supernatant (PNS) were floated on discontinuous sucrose density gradients (0.5 ml, 55%; 1.5 ml, 40%; 1.5 ml, 35%; 1.5 ml, 32%; 1.5 ml, 29%; 1.5 ml, 27%; and 1.5 ml, 20% [all wt/vol] in 1 mM EDTA–20 mM Tris base, pH 7.8) and centrifuged for 90 min at 192,000 × *g* at 4°C. ER-enriched fractions (35%–40% and 40%–55% interface bands) from the supernatant gradient were pooled, pelleted for 2 h at 190,000 × *g* at 4°C, and suspended in PBS containing 0.2 μM PMSF and 1 μl/ml protease inhibitor cocktail set III for storage at –80°C. The PNS-derived PM fractions (27%–29%, 29%–32%, and 32%–35% interface bands) were pooled, sonicated briefly (three 1-s pulses at 5-s intervals in a Misonix sonicator with a cuphorn attachment at power level 3), and added to a slurry of ConA-Sepharose 4B prewashed in buffer 1 (0.14 M KCl, 0.01 M HEPES, 1 mM MgCl₂, and 1 mM MnCl₂ [pH 7.8] with KOH). The PM-containing slurry was mixed for 2 min by nitrogen bubbling, incubated for 10 min at RT for binding, transferred to a glass preparative column, and washed with 75 ml of buffer 1. Buffer 2 (0.5 M α-methyl-mannopyranoside in buffer 1) was added and mixed by nitrogen bubbling, and the ConA-binding material was drained from the column. Fluid from a total of six sequential washes each with 14 ml of buffer 2 was collected and centrifuged for 14 h at 111,000 × *g* at 4°C, and the resulting caveolar membrane pellets were suspended in small volumes of buffer 2 for protein quantification or in buffer 2 containing 0.2 μM PMSF and 1 μl/ml protease inhibitor cocktail set III for storage at –80°C.

Protein quantification. Micro bicinchoninic acid (BCA) protein assay and SilverSNAP Stain II kits (Pierce) were used to quantify the protein concentrations in the isolated membrane fractions. The Micro BCA kit was used with bovine serum albumin standards per the manufacturer's protocol to calculate an initial protein concentration for each membrane fraction. To ensure that differences in sample solvents did not alter the analysis of marker enrichment, equal amounts of each fraction calculated as described above were resolved by sodium dodecyl sulfate-polyacrylamide gel electrophoresis (SDS-PAGE) and silver stained using SilverSNAP. Densitometry scans of the stained proteins in each lane were used to correct the BCA protein concentrations based on the difference (*n*-fold) from the lysate (Triton X-100 fractions) or homogenate (CSC fractions) absorption units.

EM of isolated caveolae. CSC caveolae were negatively stained with 2% phosphotungstic acid, pH 7.0, as described previously but with slight alterations and were examined by electron microscopy (EM) with a Zeiss EM 10C (16). In brief, CSC caveolae were adsorbed onto a Formvar-coated film grid (Electron Microscopy Sciences, Fort Washington, PA) for 1 h at RT. The adsorbed sample was stained with phosphotungstic acid, and images were captured at an 8,000-fold magnification. The captured images were scanned and processed with ImageJ (developed at the National Institutes of Health and available at <http://rsb.info.nih.gov/ij>) for scale (threefold digital zoom for a resolution of 1.52 pixels per nm), threshold, and manual discrete object separation. The processed images were analyzed in Adobe Photoshop by using Feret's function to quantify the maximum diameter of visible discrete membranes.

Endoglycosidase reactions. For endo H cleavage, 1-μg aliquots of total protein from fractionated caveolae isolated from uninfected MDCK cells and RV-infected (MOI of 2 PFU/cell) MDCK cells at 24 h postinfection (hpi) were used. The glycoproteins were denatured and diluted per the protocol of the manufacturer (New England Biolabs). Either 1 μl of sterile water (mock cleavage) or 1 μl of endo H was added to the control or sample set from mock-infected and infected cells. The cleavage reaction was performed for 1 h at 37°C, and the proteins were resolved by SDS-PAGE and visualized by Western blotting.

Western blot analyses. A series of Western blots were utilized to monitor the enrichment of each of the isolated membrane fractions with specific organelle markers and to identify those fractions containing NSP4. Two micrograms of total protein from each fraction (or 1 μg of each glycosidase-cleaved sample) was resolved on a 12% polyacrylamide minigel and transferred onto a nitrocellulose filter (0.45-μm pore size; pure nitrocellulose [GE Osmonics]) according to the directions of the manufacturer of the minigel system (Mini-PROTEAN II or Trans-Blot, respectively; Bio-Rad). The filters were blocked in 10% (wt/vol) nonfat dry milk in PBS (10% BLOTTO) for 1 h at RT, and the contents were allowed to react with the primary antibody in 2.5% BLOTTO for 14 h at 4°C with rocking. The filters were incubated for an additional 1 h at RT with the primary antibody and then washed once in 0.5% BLOTTO, twice in 0.5% BLOTTO with 0.05% Tween 20, and once in 0.5% BLOTTO with rocking (10 min per wash). Secondary antibodies were diluted in 2.5% BLOTTO and incubated with the

filters for 1 h at RT with rocking. The filters were washed as described above and rinsed with PBS, and the contents were allowed to react with SuperSignal West Pico or Femto chemiluminescent substrates per the protocols of the manufacturer (Pierce). The marker-specific bands were visualized by exposure to and development of X-ray film, and the resulting signals were analyzed by densitometry scanning.

Cholera toxin-G_{M1} binding assay. A dilution series of purified G_{M1} (0 to 100 ng) and equal amounts of total protein from the isolated fractions were spotted onto nitrocellulose filters, air dried, and rinsed twice in PBS. The filters were blocked in 3% (wt/vol) bovine serum albumin in PBS for 30 min at RT, rinsed twice gently with PBS, and incubated with 1 μg/ml CT-B in PBS for 2 h at RT. Excess CT-B was removed with two PBS rinses, and the filters were incubated with 1:500 rabbit anti-CT-B in PBS for 1 h at RT. Following two rinses with PBS, the filters were incubated with goat anti-rabbit IgG conjugated to alkaline phosphatase in PBS (1:7,500) for 30 min at RT and then rinsed twice in PBS. The filters were washed in alkaline phosphatase reaction buffer (1 M Tris, 0.1 mM NaCl, 10.5 mM MgCl₂, pH 9.0) for 5 min at RT, and the G_{M1}-CT-B signals were developed in BCIP-nitroblue tetrazolium chloride. The filters were rinsed twice in water, dried, and laminated before the analysis of the resulting signals by densitometry scanning.

Confocal microscopy. Mock- and SA11-infected MDCK cells were grown on glass coverslips and processed at 7.5 or 24 hpi for fluorescence imaging. The infected cells were rinsed in PBS and fixed and permeabilized in methanol-acetone (1:1, vol/vol) for 10 min at –20°C, and nonspecific binding sites were blocked with 3% BLOTTO (3% dry milk in PBS) at RT for 45 min. The infected and uninfected cells were incubated with primary antibodies (NSP4 and caveolin-1 peptide-specific, affinity-purified IgG) diluted in 1% BLOTTO–PBS at RT for 45 min. The cells were washed four times in 0.5% BLOTTO–PBS for 10 min each and incubated with Cy2-, Texas Red-, or Cy5-labeled secondary antibody diluted in 1% BLOTTO–PBS for 45 min in the dark. The cells were washed as described above but in the dark and mounted with fluorescent mounting medium (KPL, Inc.) onto glass slides. The resulting fluorescent images were captured with an MRC-1024MP Bio-Rad laser scanning confocal microscopy system (Bio-Rad, Hercules, CA) using an inverted Axiovert microscope (Carl Zeiss, Inc., Thornwood, NY), a 63× Zeiss oil apochromat objective, and the 488-, 568-, and 647-nm-wavelength excitation lines of an argon/krypton ion laser source. LaserSharp 3.0 (Bio-Rad), Confocal Assistant 4.02 (Brelje TC/Bio-Rad), and Adobe Photoshop 7.0 (Adobe Systems Inc., San Jose, CA), respectively, were used to capture the pixelated fluorescence data and to adjust contrast curves to construct the final images.

Indirect immunofluorescence with digital imaging. Following the transfection of HT29.f8 and MDCK cells with the pcDNA3.2D NSP4_{1–175} plasmid, cells were fixed and permeabilized (as described above) and blocked with BLOTTO (2% powdered milk in PBS) with rocking overnight at 4°C. After blocking, the cells were probed with mouse anti-NSP4_{150–175} and rabbit anti-caveolin-1 at RT for 30 min with rocking. The cell monolayers were washed four times (10 min each) with PBS, treated with goat anti-rabbit IgG-Texas Red and goat anti-mouse IgG-FITC, covered with aluminum foil, and incubated at room temperature for 30 min with rocking. Following a single rinse in PBS, the cells were stained with Hoechst 33342 to visualize the nuclei and the wash was repeated. The coverslips were air dried, mounted inverted on a microscope slide by using mounting solution, and sealed with emvelo. To examine the distribution of NSP4 when expressed alone and the colocalization of caveolin-1 with NSP4_{1–175}-transfected MDCK and HT29.f8 cells, fluorescent molecules were visualized using a Stallion digital imaging workstation (Carl Zeiss MicroImaging, Inc., Thornwood, NY) equipped with a 300-W xenon fluorescent light source with rapid switching (<2 ms) between excitation wavelengths. Images were collected using a 63× objective with a 0.75 numerical aperture and a ROPER CoolSnap HQ camera. The Stallion system filter set includes excitation and emission lines suitable for color staining with stains including DAPI (4',6'-diamidino-2-phenylindole)/Hoechst (365:445/50 nm), FITC/Cy2 (470/20:505 to 530 nm), and Texas Red/Cy3 (560/40:590 nm). The images were processed using Image J (public domain software from NIH Image).

FRET by acceptor photobleaching. FRET is a process by which nonradiative-energy transfer from one fluorophore to another occurs if the two fluorophores (or proteins) are within 10 nm of each other (25). Acceptor photobleaching is one of the simpler and more effective FRET techniques whereby the acceptor fluorophore is bleached and then an increase in the donor fluorophore is assessed to determine if two proteins interact (24). RV-infected HT29.f8 cells were labeled with Cy3-linked NSP4_{150–175} Fab and caveolin-1-specific IgG, followed by Cy2-linked secondary antibody. A series of images were taken both before (488 and 568 nm; 10% power) and after the photobleaching of the Cy3 fluorophore. The cells were photobleached at 568 nm at 100% power for 3 min. An

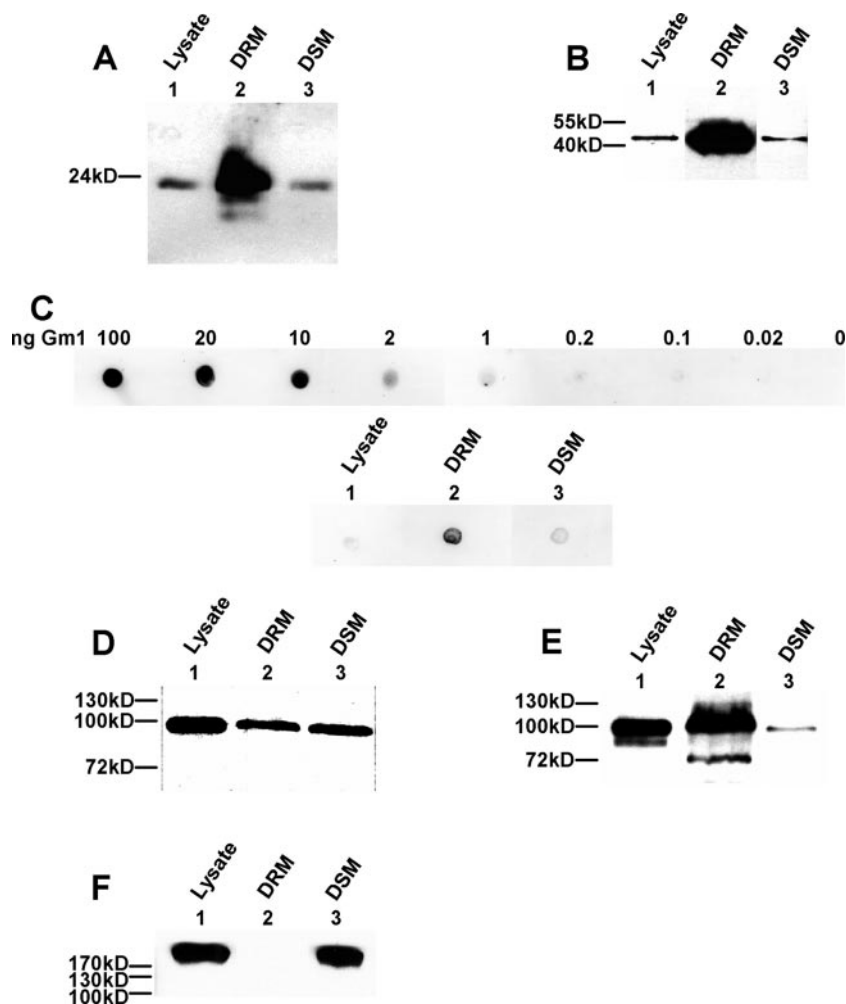


FIG. 1. Distribution of intracellular protein and lipid markers in Triton X-100-extracted membrane (DRM) fractions. Equal amounts of total protein from the cell lysate, DRM, and DSM fractions of MDCK cells were assayed for the presence of specific cellular markers (Table 1) by Western blotting. Peptide-specific antisera were used to detect caveolin-1 (A) and flotillin-1 (B). (C) CT-B and CT-B-specific antisera were used to detect the levels of the caveola-localized lipid G_{M1} by dot blotting. (D, E, and F) Marker-specific antisera identified the distribution of contaminating ER membrane (calnexin) (D), non-lipid raft PM (Na/K-ATPase α subunit) (E), and clathrin coats (clathrin heavy chain) (F).

increase in the Cy2 signal (488 nm) was assessed following photobleaching to determine if the two fluorophores were in close proximity (less than 10 nm apart) and there was a positive FRET reaction (24). Image analysis was accomplished using ImageJ software, a public domain Java image-processing program inspired by NIH Image. ImageJ has a large and increasing number of plug-ins, which are functional programming updates to ImageJ designed to perform a specific task. The FRETcalc plug-in (<http://rsb.info.nih.gov/ij/plugins/fret/fret-calc.html>) was utilized to assess the FRET data, as this plug-in is specific to acceptor photobleaching.

RESULTS

Triton X-100-resistant lipid rafts. NSP4 expression at 12 hpi has been detected in both Triton X-100-resistant and -soluble fractions isolated from RV-infected Caco-2 cells (49). To examine the DRM fraction for the presence of full-length NSP4, the resistant fraction should contain caveola-specific markers without detectable ER or nonraft PM markers. The presence of even a trace of contamination from the ER, a known reservoir of NSP4 during RV infection, in the raft/caveola fraction

may introduce NSP4 as an artifact of the isolation methodology. For analyses of the detergent-resistant and -soluble membrane fractions isolated from MDCK cells, DRM were extracted using Triton X-100. Equal amounts of lysate, DRM, and DSM proteins (Fig. 1, lanes 1 to 3, respectively) were resolved by SDS-PAGE and assayed by Western blotting for each caveola/raft and noncaveolar marker. Caveola markers, caveolin-1 (47, 50, 55) (Fig. 1A), flotillin-1 (7, 38) (Fig. 1B), and G_{M1} (42) (Fig. 1C) were present in the DRM fractions. A densitometry analysis of the caveolin-1 bands indicated that the DRM fractions were enriched approximately 3.5-fold with the key caveola protein caveolin-1 compared to the lysate (data not shown). However, the contaminant marker profiles revealed that calnexin (ER marker) (Fig. 1D) (13, 23, 45) and Na/K-ATPase α (nonraft PM marker) (Fig. 1E) (18, 30, 39, 64) were also present in the DRM fraction. The presence of ER and nonraft PM markers precluded the use of DRM for determining if full-length NSP4 traffics to PM caveolae.

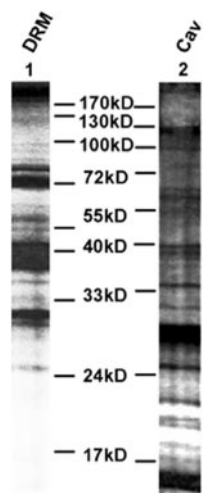


FIG. 2. Silver stain analysis of DRM and CSC caveolae. Equal amounts of total protein from Triton X-100-extracted DRM and isolated CSC caveolae (Cav) were resolved by 12% SDS-PAGE and evaluated by silver staining.

Isolation of PM-enriched caveolae from epithelial cells in the absence of an ER or nonraft PM marker. The recovery of PM-enriched material was optimized for MDCK cells by a previously reported nitrogen cavitation and sucrose gradient fractionation technique (15). These PM fractions were utilized to isolate caveolae free of contaminants relative to NSP4, in particular, ER contaminants. Following cell homogenization, the nuclei and intact cells were pelleted and the PNS was fractionated on discontinuous sucrose gradients. Equal volumes of sequential fractions from the gradient were resolved by SDS-PAGE and examined by Western blotting for the presence of caveolin-1, Na/K-ATPase α , and calnexin (data not shown). The resulting marker profiles indicated that the gradient layers between the 27% and 29% sucrose interface and the 32% and 35% sucrose interface were enriched with both caveola and PM markers, with a minimal amount of an ER marker. This PM-enriched fraction was briefly sonicated to disrupt large membrane sheets, further purified by ConA affinity chromatography, tested for caveola and noncaveola markers, and designated CSC caveolae.

Differential protein composition and membrane structure in DRM and CSC caveola fractions. To determine if the global protein composition of the CSC caveola fraction was similar to that of the DRM fraction, equal amounts of Triton X-100-extracted and CSC-isolated membrane fractions were resolved by SDS-PAGE and examined by silver staining. As anticipated, there were distinct banding patterns for both DRM and CSC caveolae, with unique and similar bands at different molecular masses (Fig. 2). The predominant DRM bands were present at 24 kDa and above, while the major bands of CSC caveolae were below 24 kDa. Hence, there was a striking difference in the overall protein contents of the DRM and CSC caveolae.

EM images of CSC caveolae showed vesicular membrane structures (Fig. 3A) with an average diameter of 99 nm ($n = 61$). The separation of these structures into groups of objects with diameters within a 10-nm range showed that a majority of these isolated membranes had diameters within the expected

range for intact caveolae (50 to 100 nm) or appeared to be smaller, broken structures (Fig. 3B).

CSC-isolated caveolae contained caveola markers in the absence of detectable ER and nonraft PM markers. To test for the presence of caveola, ER, and nonraft PM markers in the CSC caveolae, equal amounts of homogenate, PNS, ER, PM, and CSC caveola fractions were resolved by SDS-PAGE and analyzed by Western or dot blotting for the corresponding cellular markers (Table 1). Specific bands corresponding to caveolin-1 and flotillin-1 and spots specific for G_{MI} confirmed the presence of each caveola marker in the CSC caveolae (Fig. 4A to C). The contaminant marker profiles (Fig. 4D to F) showed that the protein composition of CSC caveolae differed from that of DRM isolated from the same cells (Fig. 1). The absence of calnexin in CSC caveolae (Fig. 4D) demonstrated that the CSC isolation method yielded membranes lacking the detectable ER contamination endemic in the DRM technique. Thus, the CSC caveola preparation was more suitable for our studies to detect NSP4 in PM caveolae. The relatively intense bands corresponding to clathrin (26, 52, 59) and Na/K-ATPase α in the CSC PM fraction and the absence of detectable amounts of either protein in CSC caveolae indicated that these noncaveolar protein markers were absent in the final CSC caveola fraction isolated from the PM-enriched material (Fig. 4E and F).

RV infection did not affect marker distributions in CSC caveolae. To ensure that the presence of NSP4 in CSC caveolae was not due to the redistribution of ER or nonraft membranes into the caveola fraction by viral infection, CSC fractions were isolated from RV-infected MDCK cells at 24 hpi and analyzed by Western blotting for the same protein markers (Table 1). The caveola marker profiles showed that the infected CSC caveolae contained both caveolin-1 and flotillin-1 (Fig. 5A and B) but lacked calnexin (Fig. 5C). Since clathrin and Na/K-ATPase α were also absent in the infected CSC caveola fraction (Fig. 5D and E), RV infection did not redistribute intracellular organelles or nonraft PM into the CSC caveolae at the time point examined. These data indicated that if NSP4 was present in the infected CSC caveolae, its presence would be not from cross-contamination with other intracellular organelles but from the transport of NSP4 to PM caveolae.

Full-length, endo H-sensitive NSP4 was present in CSC caveolae isolated from RV SA11-infected epithelial cells. To evaluate the presence of NSP4 in PM caveolae during RV infection, CSC fractions were isolated from mock- or RV-infected MDCK cells, resolved by SDS-PAGE, and analyzed by Western blotting. NSP4-specific bands were present at 28, 24, and 20 kDa, the expected molecular masses of doubly, singly, and unglycosylated full-length enterotoxin, in the homogenate, and the ER and PM fractions were enriched with NSP4-specific bands (Fig. 6A, lanes 6, 8, and 9, respectively) (14). Of these NSP4 bands, the 28-kDa NSP4 band was present in CSC caveolae and the 24- and 20-kDa bands were absent (Fig. 6A, lane 10). A smaller protein of approximately 16 kDa was also visible in all preliminary fractions and in CSC caveolae when blots were overexposed (Fig. 6A, lane 11). This 16-kDa band was presumed to represent a single cleaved fragment (residues 42 to 175) or dimers of the 7.5-kDa NSP4 cleavage product (aa 112 to 175) (65).

The endo H sensitivity of NSP4 was used to verify that the

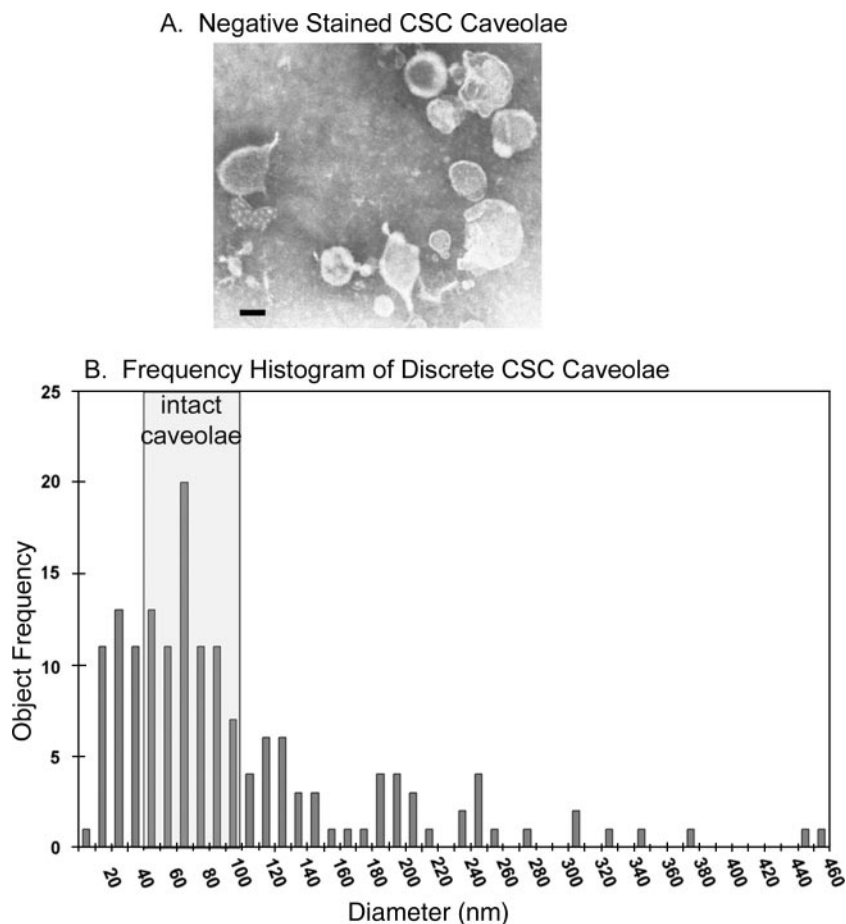


FIG. 3. EM imaging and analyses of CSC caveolae. CSC caveolae were negatively stained with 2% phosphotungstic acid and imaged by EM. (A) A threefold digital magnification was used to resolve the ultrastructure of the membranes to a resolution of 1.52 pixels per nm (bar indicates 100 nm). (B) The manual separation of discrete objects and an analysis of the maximum object diameter by Feret's function resulted in the determination of diameters in the CSC caveola fraction. The diameters were segregated into groups including all the diameters within a 10-nm range, and the representative values (*x* axis) were plotted against the number of objects observed with diameters in the corresponding range. Analyses of 161 discrete objects revealed the size distribution of the membranes in CSC caveolae.

28-kDa bands seen in the homogenate and CSC caveolae were due to the glycosylation state of NSP4 (Fig. 6B) and that both termini of NSP4 were present. The presence of the N terminus of NSP4 was established by the presence of glycosylation sites (at aa 8 and 18), and that of the C terminus was confirmed by using a C-terminal peptide-specific antibody (anti-NSP4₁₅₀₋₁₇₅)

(9). endo H pretreatment of the infected homogenate resulted in a significant loss of the 28-kDa NSP4-specific band, with a coinciding increase in the intensity of the 20-kDa (unglycosylated) NSP4 band (Fig. 6B, lanes 5 and 6). In addition, endo H pretreatment of the CSC caveolae resulted in a shift of the NSP4 28-kDa band to the unglycosylated, 20-kDa form (Fig.

TABLE 1. Intracellular organelle and membrane markers

Marker	Subcellular distribution	Comment(s)	Reference(s)
Caveolin-1	Caveolae, ER, Golgi apparatus	Defining caveola marker; hairpin structure with C and N termini exposed	47, 50, 55
Flotillin-1	Lipid rafts	Potentially involved in caveola localization; peripheral membrane protein	7, 38, 58
Ganglioside M1	PM caveolae	Glycolipid; primary cholera toxin receptor	42
Calnexin	ER	Integral membrane protein; ER chaperone	13, 23, 45
Giantin	<i>cis</i> -medial Golgi network	Integral membrane protein	29
Golgin-97	<i>trans</i> -Golgi network	Peripheral membrane protein	13, 18, 32
Na/K-ATPase α subunit	Nonraft PM	Integral membrane protein; one reporter of caveola localization in cardiac cells	30, 39, 64
Clathrin heavy chain	PM-coated pits, <i>trans</i> -Golgi network, endosomes	Membrane-association protein	26, 52, 59

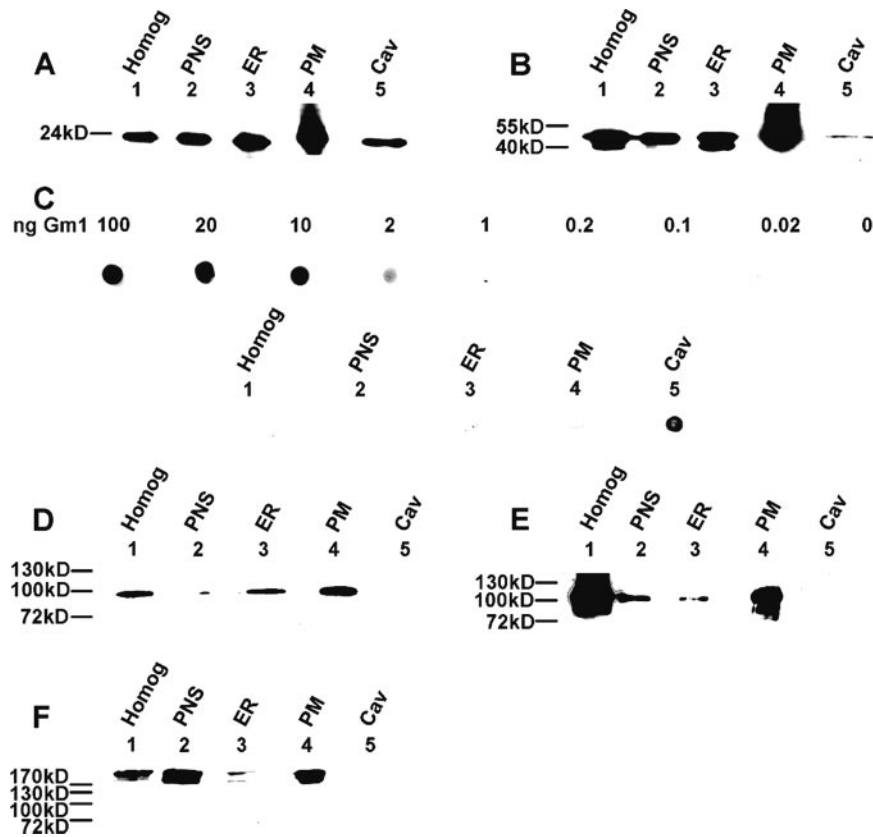


FIG. 4. Distribution of intracellular protein and lipid markers in CSC-isolated membrane fractions. Equal amounts of total protein from homogenate (Homog), PNS, ER, PM, and caveola (Cav) fractions isolated from MDCK cells by CSC isolation were assayed for the presence of the corresponding markers (Table 1). Peptide-specific antisera were used to detect caveolin-1 (A) and flotillin-1 (B) by Western blotting. (C) CT-B and CT-B-specific antisera were used to detect the levels of the caveola-localized lipid G_{M1} by dot blotting. (D, E, and F) Marker-specific antisera and Western blots identified the distribution of contaminating ER membrane (calnexin) (D), non-lipid raft PM (Na/K-ATPase α subunit) (E), and clathrin-coated membranes (clathrin heavy chain) (F) in each of the membrane fractions.

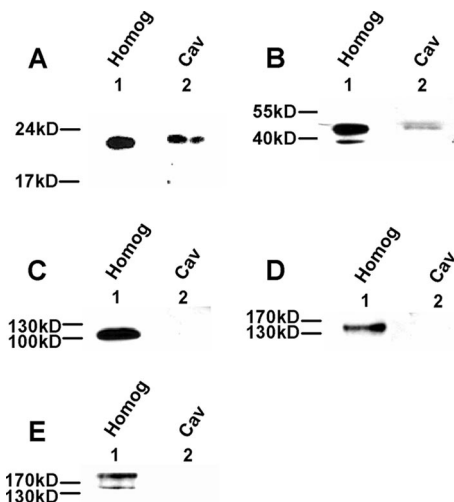


FIG. 5. Distribution of the intracellular markers in CSC caveolae from RV-infected cells. Equal amounts of total protein from homogenate (Homog) and caveola (Cav) fractions isolated from RV-infected MDCK cells were assayed for a panel of cellular markers (Table 1). Peptide-specific antisera were used to detect caveolin-1 (A) and flotillin-1 (B) by Western blotting. Marker-specific antisera and Western blots were used to identify the distribution of contaminating ER membrane (calnexin) (C), non-lipid raft PM (Na/K-ATPase α subunit) (D), and clathrin-coated membranes (clathrin heavy chain) (E) in each membrane fraction.

6B, lanes 7 and 8). The smaller, 16-kDa band was unaffected by endo H digestion (data not shown). The absence of the singly glycosylated NSP4 form and the presence of the unglycosylated 16-kDa fragment in the CSC caveolae indicated that the inclusion of full-length, doubly glycosylated NSP4 in the PM caveolae was not due to NSP4 glycans' simply binding ConA.

NSP4 associates with caveolin-1 but not Golgi apparatus-localized proteins at early and late stages of RV infection. The endo H sensitivity of NSP4 in CSC caveolae isolated from MDCK cells at 24 hpi suggested that the enterotoxin bypassed the endomannosidase-rich Golgi apparatus during transport from the ER (17, 22, 28, 37). We therefore examined RV-infected MDCK cells for the colocalization of NSP4 and caveolin-1 at 7.5 and 24 hpi. Confocal imaging demonstrated the association of NSP4 with caveolin-1 at both the early and late time points postinfection (Fig. 7, colored panels). An examination of the subcellular distribution of NSP4 in RV-infected MDCK cells revealed the presence of NSP4 at perinuclear sites, in cytoplasmic vesicular-like structures, and at the cell periphery (Fig. 7) and an increase in the NSP4 signal at 24 hpi compared to that at 7.5 hpi. In contrast, the levels of the caveolin-1 signal at both time points appeared to be essentially the same. Similarly, colocalization at the cell periphery and in

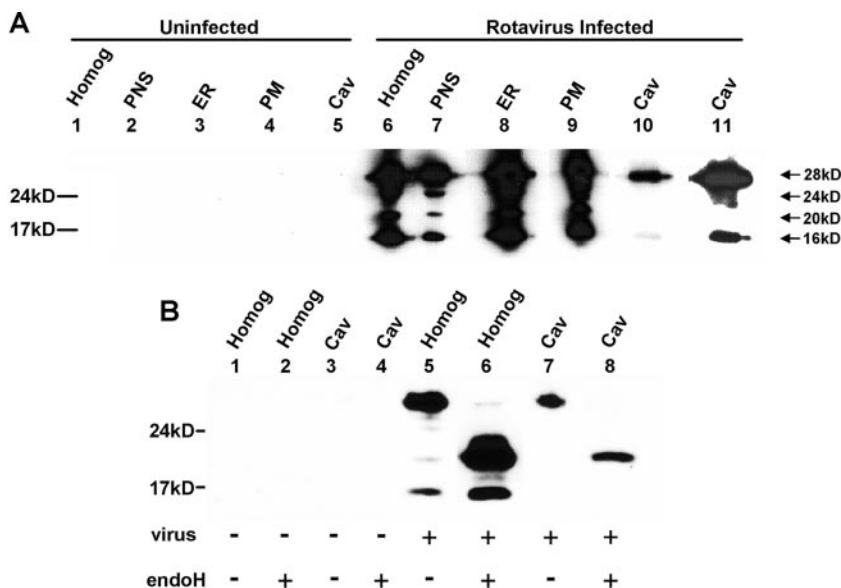


FIG. 6. Detection of full-length, endo H-sensitive NSP4 in CSC caveolae isolated from RV-infected MDCK cells. (A) Equal amounts of total protein from homogenate (Homog), PNS, ER, PM, and CSC caveola (Cav) fractions from mock- and RV-infected MDCK cells were assayed for the presence of NSP4 with NSP4₁₅₀₋₁₇₅-specific antisera. Homogenate, PNS, ER, and PM fractions showed NSP4-specific banding profiles consistent with doubly, singly, and unglycosylated full-length NSP4 (28, 24, and 20 kDa, respectively) in addition to a ~16-kDa band that may be a dimer of the NSP4 cleavage fragment (aa 112 to 175). CSC caveolae (lane 10) contained predominately the doubly glycosylated, 28-kDa form of NSP4, with a relatively small amount of the 16-kDa band observed when the film was significantly overexposed (lane 11). (B) The homogenate and CSC caveola (lanes 3 and 4) fractions from uninfected cells were mock- and endo H-treated to determine if the enzyme treatment altered the specificity of NSP4 staining demonstrated in panel A. The homogenate and CSC caveolae from RV-infected MDCK cells were similarly mock- or endo H-treated to confirm that the multiple forms of NSP4 were due to differences in the glycosylation state of the full-length protein and the absence of Golgi apparatus-specific mannosidase trimming. +, present; -, absent.

vesicular-like structures in the cytoplasm was seen (Fig. 7, right panels). At the same times postinfection, the association of giantin, a *cis*-medial Golgi network marker, and NSP4 was evaluated (data not shown). These data revealed an absence of colocalization with the *cis*-medial Golgi network marker, in agreement with a recent report showing that NSP4-enhanced green fluorescent protein (EGFP) and giantin fail to colocalize (6). The specificity of each antibody set was corroborated using mock-infected cells, as well as secondary antibody controls (Fig. 7, top panels).

While caveolin-1 traffics directly between the ER and PM caveolae in specific chaperone complexes, the only experimentally defined caveolin-1 vesicular pathway transits through the Golgi apparatus and buds from the *trans*-Golgi network, albeit other vesicular pathways have been suggested, including direct transport between the ER and the PM (10, 44, 61). Therefore, the subcellular distribution of the *trans*-Golgi network-localized golgin-97 (13, 32) in CSC-isolated membrane fractions was examined by Western blotting (Fig. 8). Analogous to the lack of NSP4 colocalization with a *cis*-medial Golgi network marker, there was an absence of golgin-97 in the caveola fraction (Fig. 8, lane 5). Hence, fluorescence imaging and Western blotting failed to detect *cis*-medial and *trans*-Golgi network markers, respectively.

NSP4 expression was sufficient for colocalization with caveolin-1. To determine if additional viral proteins were required for the intracellular NSP4-caveolin-1 association, epifluorescence was utilized with NSP4-transfected cells. In the absence of other viral proteins, NSP4 had the same subcellular

distribution patterns in both MDCK and HT29.f8 cells as those observed during RV infection (Fig. 9, central panels). Both cell lines stained for caveolin-1, whereas only one of the HT29.f8 cells (of the two shown) was transfected, as indicated by the presence of NSP4 (Fig. 9, upper panels). Additionally, the NSP4 and caveolin-1 proteins in the transfected cells colocalized (Fig. 9, far-right panels) at intracellular sites similar to those observed in RV-infected cells (compare Fig. 7). These results confirmed that the NSP4 protein is sufficient in and of itself to associate with the key caveolar structural protein caveolin-1 in two different cell types.

NSP4-caveolin-1 association was resolved to within a 10-nm radius in MDCK cells during RV infection. The colocalization of NSP4 and caveolin-1 during RV infection or NSP4 transfection resolved the proteins to within about 200 nm, whereas FRET analyses with Cy2- and Cy3-labeled probes resolved the NSP4-caveolin-1 interaction to an area of less than 10 nm in radius (Fig. 10, boxes 1) (48). Figure 10A and B show the labeled NSP4 (acceptor) before and after photobleaching (large boxes) in MDCK cells. Likewise, panels C and D illustrate the caveolin-1 (donor) signal prior to and after the photobleaching of the acceptor. The caveolin-1 donor (Cy2) signal emission increased by 7.83% (Table 2) and was FRET strongly positive in areas where NSP4 was extensively bleached (Fig. 10, boxes 1). Cells in the control areas of the same fields of view, where NSP4 was only partially bleached (boxes 2) or where NSP4 was not present (boxes 3), failed to show an increase in the donor (caveolin-1) signal (Table 2). As anticipated, those areas corresponding to boxes 2 and 3 showed weak or negative

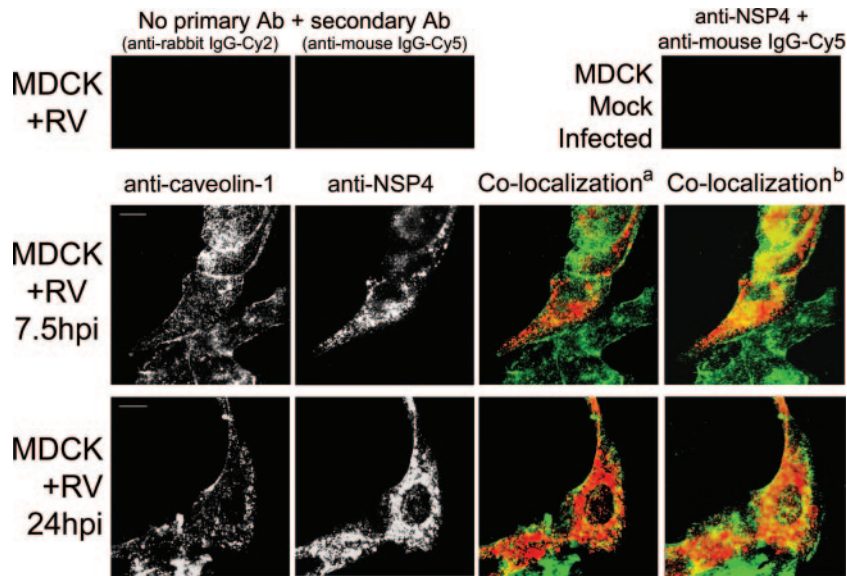


FIG. 7. Association of NSP4 with caveolin-1 during early and late rotavirus infection. RV-infected MDCK cells were probed with the indicated primary antibodies. Fluorescently tagged secondary antibodies were imaged with 488-nm- and then 647-nm-wavelength excitation sources to capture Cy2 and Cy5 data, respectively, and to control for Cy2 signal bleed-through into the Cy5 images. Images from mock (right upper panel)- and RV (left and center upper panels)-infected cells in the absence of the indicated primary antibodies were used to control for the stain specificity and nonspecific binding of each antibody set. Shown are the data acquired for caveolin-1 and NSP4 and the merged images (co-localization^a; caveolin-1 is in green, and NSP4 is in red). To optimize the visualization of the relative amounts of colocalized NSP4 and caveolin-1, a merged set of 8 z-series images (taken at 0.75- μ m intervals) is also shown (co-localization^b). The images shown are representative of results from four experiments.

FRET. As the Forester radius of the Cy2-Cy3 fluorophore pair is 5 to 6 nm and the calculated probe-to-probe radius is dependent on the inverse sixth power of the intermolecular separation, the NSP4 and caveolin-1 labels must be no more than 10 nm from each other for the detection of a FRET reaction (24, 25), i.e., a positive FRET reaction placed at least some portion of the NSP4 and caveolin-1 protein pools within 10 nm of each other, highly indicative of a protein-protein interaction.

DISCUSSION

By utilizing a newly developed PM caveola isolation protocol and RV-infected MDCK cells, our data showed the presence of full-length, high-mannose glycosylated NSP4 in PM caveolae that lacked an ER marker but contained caveolin-1, flotillin-1, and G_{M1}. Several reports have implicated the association of NSP4 with lipid rafts. First, a preferential interaction between NSP4 and NSP4₁₁₄₋₁₃₅ with anionic, cholesterol-rich, caveola-like model membranes has been shown by circular

dichroism and a filter-binding assay (20, 21). Second, RV particles, VP4 (the RV spike protein), and NSP4 are associated with DRM in RV-infected cells (49). Third, infectious RV particles and NSP4 are detected in Triton X-100-insoluble fractions and are sensitive to drugs that compromise lipid raft integrity (12). Fourth, NSP4 directly binds caveolin-1, with the binding site mapping to NSP4 residues 114 to 135 (41). Taken together, these data strongly indicate an association of raft membranes with NSP4 for intracellular transport from the ER to the PM. However, these data are inconclusive, as DRM contain a large quantity of ER-specific markers.

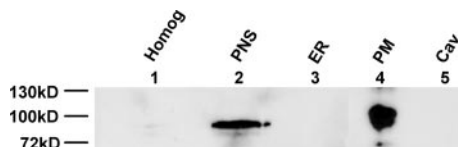


FIG. 8. Distribution of golgin-97 in CSC-isolated membrane fractions. Equal amounts of total protein from homogenate (Homog), PNS, ER, PM, and CSC caveola (Cav) fractions obtained from RV-infected MDCK cells by CSC isolation were assayed for the presence of the *trans*-Golgi network marker golgin-97. Golgin-97 in the CSC caveola fraction was undetectable by Western blotting.

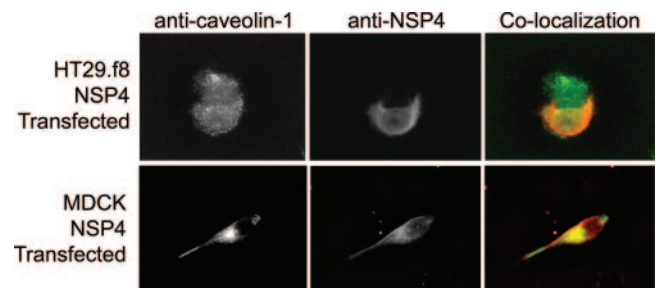


FIG. 9. Colocalization of NSP4 with caveolin-1 in transfected cells. HT29.f8 (top panels) and MDCK (bottom panels) cells were transfected with pcDNA3.2D NSP4₁₋₁₇₅ plasmid DNA and probed with the indicated primary antibodies. Fluorescently tagged secondary antibodies were imaged with 488-nm- and then 560-nm-wavelength excitation sources to capture Cy2 and Texas Red signals, respectively ($n = 4$). Caveolin-1 (left panels) and NSP4 (center panels) distributions are shown. Note that only one of the two HT29.f8 cells shown was transfected (NSP4 signal). The panels on the far right are merged images showing the colocalization of NSP4 (red) and caveolin-1 (green).

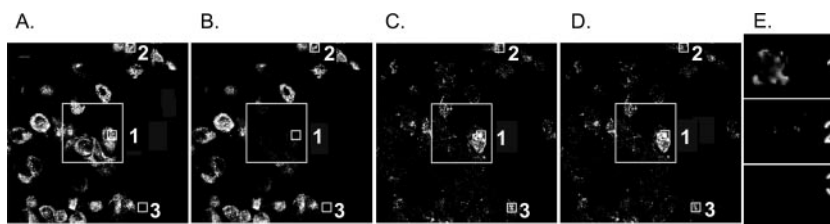


FIG. 10. FRET analysis by acceptor photobleaching. NSP4 was probed with Cy3-linked Fab prepared from anti-NSP4₁₅₀₋₁₇₅ IgG and caveolin-1 was probed with anti-caveolin-1 followed by Cy2-conjugated goat anti-rabbit antibody in RV-infected HT29.f8 cells. The Cy3 and Cy2 images were acquired with the 568-nm- and 488-nm-wavelength lasers (panels A and C are prebleach images of NSP4 and caveolin-1, respectively). Subsequently, an area highlighted by the large boxes in panels A to D was photobleached with the 568-nm-wavelength laser at 100% power for 3 min. Cy3 and Cy2 signals were reimaged following the photobleaching of the acceptor signal (panels B and D are postbleach images of NSP4 and caveolin-1). Panel B demonstrates the efficient photobleaching of the acceptor within the large box. To monitor FRET efficiency, three small areas were selected and closely examined for FRET (box 1, area where NSP4 was extensively bleached; box 2, area where NSP4 was partially bleached; and box 3, area where NSP4 was not present). On the far right (panel E), images corresponding to the small boxes are enlarged to visualize the percentage of FRET that varied from no signal when NSP4 was absent (box 3) to a significant amount when NSP4 was bleached (box 1).

There are several reported raft/caveola isolation protocols that have been extensively utilized to study the compositions and interactions specific to raft membrane microdomains (43, 44). For our purposes, it was critical to isolate PM caveolae free of even a trace of ER contamination. The ER is a known reservoir of NSP4 during RV infection, and the presence of ER membranes could nonspecifically introduce NSP4 into caveolae in the absence of NSP4-raft association (5). We recognize that this concern may be unique to NSP4 and other ER-localized proteins in that a trace of ER contamination would not influence the conclusions of other studies.

A recent report has revealed that NSP4 bypasses the Golgi apparatus en route from the ER to the cell periphery by using an NSP4-EGFP fusion protein (6). In that study, the NSP4-EGFP fusion protein failed to localize with the Golgi apparatus marker, giantin, but colocalized with the autophagosomal marker LC3 and accumulated close to, but not within, the PM cytoplasmic leaflet. In the present study, we show fully glycosylated, endo H-sensitive NSP4 in CSC caveolae. This discrepancy in PM localization may be due to inherent differences in virally expressed NSP4 versus NSP4 expressed with a large fusion partner (EGFP) or the use of alternate analysis techniques. Nonetheless, our data agreed with the results of a study by Berkova et al. (6) on several key points, including the presence of NSP4 in cytoplasmic, vesicular-like structures that bypass the Golgi apparatus during transport to the cell surface and the presence of non-ER NSP4 intracellular pools with apparently distinct functions.

Caveolae can function as vesicular carriers containing key fusion complex proteins that mediate vesicle formation, dock-

ing, and fusion, including GTPases, annexins, *N*-ethylmaleimide-sensitive fusion factor, soluble *N*-ethylmaleimide-sensitive fusion factor attachment proteins, and soluble *N*-ethylmaleimide-sensitive fusion factor attachment protein receptors (46, 53, 54). It remains unclear if CSC caveolae interact with fusion-competent caveola vesicles. The autophagosomes carrying NSP4 apparently do not fuse with other membranes such as the PM (6). Hence, distinct, functionally divergent NSP4 pools may be uniquely transported, as suggested by Berkova et al. (6).

NSP4 and caveolin-1 colocalized at multiple sites within infected cells (this study and reference 41). Although colocalizations via the merging of confocal images are widely used to determine if two or more molecules are in close proximity, the resolution of the positions of these colocalized molecules is approximately within 200 nm (35). Given that caveolae are 50 to 100 nm in diameter, imaging data alone are unconvincing, necessitating a second, confirmatory technique. Hence, we evaluated the composition of caveolae (free of ER contaminants) and performed FRET analyses of NSP4 and caveolin-1, bringing the resolution to within 10 nm (48).

Caveolin-1 and G_{M1} are established markers for raft/caveola fractions (47, 56, 58). Flotillin-1, a 45-kDa membrane-associated protein enriched with isolated lipid rafts as defined by Triton X-100-extracted DRM, is also detected in sodium carbonate (high pH)-extracted caveolae but is absent from immunopurified caveolae (7, 38, 58). In our hands, flotillin-1 was present in CSC caveolae along with the other two caveola markers, although the CSC caveolae were not enriched with protein markers compared to the PM. Our focus was on obtaining pure, ER-negative PM caveolae rather than acquiring

TABLE 2. Mean fluorescence values from FRET analyses^a

Photoacceptor status	Mean fluorescence value for NSP4		Mean fluorescence value for caveolin-1		% Change in caveolin-1 mean fluorescence ^b
	Prebleach	Postbleach	Prebleach	Postbleach	
Bleached with 100% power	111	4	115	124	7.8
Bleached with 32% power	107	73	65	46	-29.2
Not present	0	0	71	46	-35.2

^a Mean fluorescence intensities are expressed in arbitrary units as acquired from ImageJ. Data correspond to boxes 1 (bleached with 100% power), 2 (bleached with 32% power), and 3 (not present) in Fig. 10A to D.

^b Amount of increase or decrease (-) in Cy2-labeled caveolin-1 after bleaching of Cy3-labeled NSP4.

large quantities of raft membranes. We discovered that there was a trade-off between purity and recovery, with a probable loss of some portion of the PM caveolae during processing. Alternatively, the brief sonication used to disrupt the large membrane sheets before ConA affinity isolation may have sheared a portion of the peripheral and membrane-associated protein populations. In that instance, the presence of full-length NSP4 in CSC caveolae would suggest that NSP4 crosses the PM bilayer rather than interacting through a peripheral association. Additional studies are needed to distinguish these precise protein-lipid interactions.

To ensure that the presence of NSP4 in CSC caveolae was not due to the coisolation of a contaminant membrane, calnexin (ER), golgin-97 (Golgi apparatus), clathrin (clathrin-coated pit), and Na/K-ATPase α (nonraft PM) marker proteins were examined. These proteins are commonly utilized to indicate the presence of the corresponding membranes in cell fractionation experiments due to their association with specific intracellular membranes (13, 30, 32, 45). The resultant marker profiles indicated that the CSC caveola fraction was void of detectable ER, Golgi, and clathrin-coated membranes, as well as nonraft PM domains.

The recent identification of NSP4 in DRM isolated from replicative-form RV-infected colon cells prompted us to evaluate the composition of identical DRM isolated from MDCK cells and provide further insight into the presence of NSP4 in lipid rafts and caveolae (12, 49). While clathrin was not detected in MDCK DRM, significant amounts of the ER and nonraft PM markers were present. Due to the ER and nonraft PM contaminants, the previous identification of NSP4 in DRM is indicative of, but not conclusive about, NSP4 caveola localization.

The critical intracellular receptor function of NSP4 in RV morphogenesis stresses the importance of an NSP4 pool in the ER during infection (2, 5). NSP4 in CSC caveolae extracted from a PM-enriched material devoid of detectable ER contamination indicates the presence of a second pool of NSP4 that is transported to PM caveolae during infection. Third and fourth pools present in LC3-containing autophagosomes and radiating from the ER-Golgi intermediate compartment along microtubules have been detected previously (6, 63). It is reasonable to propose that the RV multifunctional enterotoxin is transported by multiple cellular pathways to different intracellular locations due to interactions with different host molecules. Further, more than one pathway may direct NSP4 to the same intracellular site.

The visualization of NSP4 in transfected cells showed a pattern similar to that seen following a virus infection. These data indicated that NSP4 traffics to distinct intracellular locations in the absence of other viral proteins. While it remains unknown if the structure or the primary sequence of NSP4 facilitates its transport, transfected NSP4 still colocalized with caveolin-1 in the absence of other viral proteins. Positive FRET analyses further confirmed the specific interaction of NSP4 and caveolin-1 during RV infection.

In summary, NSP4 is a multifunctional, complex glycoprotein that uniquely interacts with host cell molecules. The data presented herein confirm the presence of full-length NSP4 in PM caveolae and the lack of Golgi network association in transport to the PM. Additional studies are needed to deter-

mine if NSP4 transport is dependent on caveolin-1 or caveola intracellular movement and to fully elucidate the many roles of NSP4 during infection.

ACKNOWLEDGMENTS

This research was supported by Department of Health and Human Services-National Institute of General Medical Sciences, National Institutes of Health grants GM 62326 (J.M.B.) and GM 3131651 (F.S.) and National Institutes of Health Public Health Service grant T32 AI572072-01A1 (S.M.S. and J.M.B.).

We acknowledge the contribution of H. Ross Payne for EM analyses.

REFERENCES

- Adachi, S., A. R. Cross, B. M. Barior, and R. A. Gottlieb. 1997. Bcl-2 and the outer mitochondrial membrane in the inactivation of cytochrome c during Fas-mediated apoptosis. *J. Biol. Chem.* **272**:21878–21882.
- Au, K. S., W. K. Chan, J. W. Burns, and M. K. Estes. 1989. Receptor activity of rotavirus nonstructural glycoprotein NS28. *J. Virol.* **63**:4553–4562.
- Axen, R., J. Porath, and S. Ernback. 1967. Chemical coupling of peptides and proteins to polysaccharides by means of cyanogen halides. *Nature* **214**:1302–1304.
- Ball, J. M., P. Tian, C. Q. Y. Zeng, A. P. Morris, and M. K. Estes. 1996. Age-dependent diarrhea induced by a rotaviral nonstructural glycoprotein. *Science* **272**:101–104.
- Bergmann, C. C., D. Maass, M. S. Poruchynsky, P. H. Atkinson, and A. R. Bellamy. 1989. Topology of the non-structural rotavirus receptor glycoprotein NS28 in the rough endoplasmic reticulum. *EMBO J.* **8**:1695–1703.
- Berkova, Z., S. E. Crawford, G. Trugnan, T. Yoshimori, A. P. Morris, and M. K. Estes. 2006. Rotavirus NSP4 induces a novel vesicular compartment regulated by calcium and associated with viroplasm. *J. Virol.* **80**:6061–6071.
- Bickel, P. E., P. E. Scherer, J. E. Schnitzer, P. Oh, M. P. Lisanti, and H. F. Lodish. 1997. Flotillin and epidermal surface antigen define a new family of caveolae-associated integral membrane proteins. *J. Biol. Chem.* **272**:13793–13802.
- Boshuizen, J. A., J. W. A. Rossen, C. K. Sitaram, F. F. P. Kinenai, Y. Simons-Oosterhuis, J. A. Lafferber, H. A. Büller, and A. W. C. Einerhand. 2004. Rotavirus enterotoxin NSP4 binds to the extracellular matrix proteins laminin- β 3 and fibronectin. *J. Virol.* **78**:10045–10053.
- Both, G. W., L. J. Siegman, A. R. Bellamy, and P. H. Atkinson. 1983. Coding assignment and nucleotide sequence of simian rotavirus SA11 gene segment 10: location of glycosylation sites suggests the signal peptide is not cleaved. *J. Virol.* **48**:335–339.
- Cohen, A. W., R. Hnasko, W. Schubert, and M. P. Lisanti. 2004. Role of caveolae and caveolins in health and disease. *Physiol. Rev.* **84**:1341–1379.
- Cuadras, M. A., B. B. Bordier, J. L. Zambrano, J. E. Ludert, and H. B. Greenberg. 2006. Dissecting rotavirus particle-raft interaction with small interfering RNAs: insights into rotavirus transit through the secretory pathway. *J. Virol.* **80**:3935–3946.
- Cuadras, M. A., and H. B. Greenberg. 2003. Rotavirus infectious particles use lipid rafts during replication for transport to the cell surface in vitro and in vivo. *Virology* **313**:308–321.
- Drenan, R. M., X. Liu, P. G. Bertram, and X. F. S. Zheng. 2004. FKBP12-rapamycin-associated protein or mammalian target of rapamycin (FRAP/mTOR) localization in the endoplasmic reticulum and the Golgi apparatus. *J. Biol. Chem.* **279**:772–778.
- Ericson, B. L., D. Y. Graham, B. B. Mason, and M. K. Estes. 1982. Identification, synthesis, and modifications of simian rotavirus SA11 polypeptides in infected cells. *J. Virol.* **42**:825–839.
- Gallegos, A. M., S. M. Storey, A. B. Kier, F. Schroeder, and J. M. Ball. 2006. Structure and cholesterol dynamics of caveolae/raft and non-raft plasma membrane domains. *Biochemistry* **45**:12100–12116.
- Gelderblom, H. R., H. Renz, and M. Özel. 1991. Negative staining in diagnostic virology. *Micron Microsc. Acta* **22**:435–477.
- Gottschalk, A. 1972. *Glycoproteins: their composition, structure, and function*. Elsevier Publishing Company, New York, NY.
- Gustavsson, J., S. Parpal, M. Karlsson, C. Ramsing, H. Thron, M. Borg, M. Lindroth, K. H. Peterson, K.-E. Magnusson, and P. Strålfors. 1999. Localization of the insulin receptor in caveolae of adipocyte plasma membrane. *FASEB J.* **13**:1961–1971.
- Heerklott, H., H. Szadkowska, T. Anderson, and J. Seelig. 2003. The sensitivity of lipid domains to small perturbations demonstrated by the effect of Triton. *J. Mol. Biol.* **329**:793–799.
- Huang, H., F. Schroeder, M. K. Estes, T. McPherson, and J. M. Ball. 2004. Interaction(s) of rotavirus non-structural protein 4 (NSP4) C-terminal peptides with model membranes. *Biochem. J.* **380**:723–733.
- Huang, H., S. Schroeder, C. Zeng, M. K. Estes, J. K. Schoer, and J. M. Ball. 2001. Membrane interactions of a novel viral enterotoxin: rotavirus non-structural glycoprotein NSP4. *Biochemistry* **40**:4169–4180.

22. **Hubbard, S. C., and R. J. Ivatt.** 1981. Synthesis and processing of asparagine-linked oligosaccharides. *Annu. Rev. Biochem.* **50**:555–583.
23. **Jackson, M. R., T. Nilsson, and P. A. Peterson.** 1990. Identification of a consensus motif for retention of transmembrane proteins in the endoplasmic reticulum. *EMBO J.* **9**:3153–3162.
24. **Karpova, T. S., C. T. Baumann, L. He, X. Wu, A. Grammer, P. Lipsky, G. L. Hager, and J. G. McNally.** 2003. Fluorescence resonance energy transfer from cyan to yellow fluorescent protein detected by acceptor photobleaching using confocal microscopy and a single laser. *J. Microsc.* **209**:56–70.
25. **Kenworthy, A. K.** 2001. Imaging protein-protein interactions using fluorescence resonance energy transfer microscopy. *Methods* **24**:289–296.
26. **Kirchhausen, T.** 2000. Three ways to make a vesicle. *Nat. Rev.* **1**:187–198.
27. **Kluck, R. M., E. Bossy-Wetzel, D. R. Green, and D. D. Newmeyer.** 1997. The release of cytochrome c from mitochondria: a primary site for Bcl-2 regulated apoptosis. *Science* **21**:1132–1136.
28. **Lennarz, W. J.** 1980. The biochemistry of glycoproteins and proteoglycans. Plenum Press, New York, NY.
29. **Linstedt, A. D., and H. P. Hauri.** 1993. Giantin, a novel conserved Golgi membrane protein containing a cytoplasmic domain of at least 350 kDa. *Mol. Biol. Cell* **4**:679–693.
30. **Lisanti, M. P., P. E. Scherer, J. Vidugiriene, Z. Tang, A. Hermanowski-Vosatka, Y. H. Tu, R. F. Cook, and M. Sargiacomo.** 1994. Characterization of caveolin-rich membrane domains isolated from an endothelial-rich source: implications for human disease. *J. Cell Biol.* **126**:111–126.
31. **Lopez, T., M. Camacho, M. Zayas, R. Najera, R. Sanchez, C. F. Arias, and S. Lopez.** 2005. Silencing the morphogenesis of rotavirus. *J. Virol.* **79**:184–192.
32. **Lu, L., G. Tai, and W. Hong.** 2004. Autoantigen Golgin-97, an effector of Arl1 GTPase, participates in traffic from the endosome to the trans-Golgi network. *Mol. Biol. Cell* **15**:4426–4443.
33. **Lynch, M., W. J. Shieh, K. Tatti, J. R. Gentsch, T. F. Harris, B. M. Jiang, J. Guarner, J. S. Bresee, M. Greenwald, S. Cullen, H. D. Davies, C. Trevenen, S. R. Zaki, and R. I. Glass.** 2003. The pathology of rotavirus-associated deaths, using new molecular diagnostics. *Clin. Infect. Dis.* **37**:1327–1333.
34. **Malek, M. A., A. T. Curns, R. C. Holman, T. K. Fischer, J. S. Bresee, R. I. Glass, C. A. Steiner, and U. D. Parashar.** 2006. Diarrhea- and rotavirus-associated hospitalizations among children less than 5 years of age: United States, 1997 and 2000. *Pediatrics* **117**:1887–1892.
35. **Manders, E. M. M., F. J. Verbeek, and J. A. Aten.** 1993. Measurement of colocalization of objects in dual-color confocal images. *J. Microsc.* **169**:375–382.
36. **Mitchell, D. M. A., and J. M. Ball.** 2005. Characterization of a spontaneously polarizing HT-29 cell line, HT-29/cl.f8. *In Vivo Cell Dev. Biol.* **40**:297–302.
37. **Moremen, K. W., R. B. Trimble, and A. Herscovics.** 1994. Glycosidases of the asparagine-linked oligosaccharide processing pathway. *Glycobiology* **4**:114–125.
38. **Morrow, I. C., S. Rea, S. Martin, I. A. Prior, R. Prohaska, J. F. Hancock, D. E. James, and R. G. Parton.** 2002. Flotillin-1/Reggie-2 traffics to surface raft domains via a novel Golgi-independent pathway. *J. Biol. Chem.* **277**:48834–48841.
39. **Ovchinnikov, Y. A., N. M. Luneva, E. A. Arystarkhova, N. M. Gevondyan, N. M. Arzamazova, A. Kozhich, V. A. Nesmeyanov, and N. N. Modyanov.** 1988. Topology of Na⁺, K⁺-ATPase: identification of the extra- and intracellular hydrophilic loops of the catalytic subunit by specific antibodies. *FEBS Lett.* **227**:230–234.
40. **Parashar, U. D., E. G. Hummelman, J. S. Bresee, M. A. Miller, and R. I. Glass.** 2003. Global illness and deaths caused by rotavirus disease in children. *Emerg. Infect. Dis.* **5**:565–572.
41. **Parr, R. D., S. M. Storey, D. M. Mitchell, A. L. McIntosh, M. Zhou, K. D. Mir, and J. M. Ball.** 2006. The rotavirus enterotoxin NSP4 directly interacts with the caveolar structural protein caveolin-1. *J. Virol.* **80**:2842–2854.
42. **Parton, R. G.** 1994. Ultrastructural localization of gangliosides; GM1 is concentrated in caveolae. *J. Histochem. Cytochem.* **42**:155–166.
43. **Pike, L. J.** 2005. Growth factor receptors, lipid rafts and caveolae: an evolving story. *Biochim. Biophys. Acta* **1746**:260–273.
44. **Pike, L. J.** 2003. Lipid rafts: bringing order to chaos. *J. Lipid Res.* **44**:655–667.
45. **Rajagopalan, S., Y. Xu, and M. B. Brenner.** 1994. Retention of unassembled components of integral membrane proteins by calnexin. *Science* **263**:387–390.
46. **Razani, B., S. E. Woodman, and A. P. Lisanti.** 2002. Caveolae: from cell biology to animal physiology. *Pharmacol. Rev.* **54**:431–467.
47. **Rothberg, K. G., J. E. Heuser, W. C. Donzell, Y.-S. Ying, J. R. Glenney, and R. G. W. Anderson.** 1992. Caveolin, a protein component of caveolae membrane coats. *Cell* **68**:673–682.
48. **Sabanayagam, C. R., J. S. Eid, and A. Meller.** 2005. Using fluorescence resonance energy transfer to measure distances along individual DNA molecules: corrections due to nonideal transfer. *J. Chem. Phys.* **122**:061103–061108.
49. **Sapin, C., O. Colard, O. Delmas, C. Tessier, M. Breton, V. Enouf, S. Chwetoff, J. Ouanich, J. Cohen, C. Wolf, and G. Trugnan.** 2002. Rafts promote assembly and atypical targeting of a nonenveloped virus, rotavirus, in Caco-2 cells. *J. Virol.* **76**:4591–4602.
50. **Scheiffele, P., P. Verkade, A. M. Fra, H. Virla, K. Simons, and E. Ikonen.** 1998. Caveolin-1 and -2 in the exocytic pathway of MDCK cells. *J. Cell Biol.* **140**:795–806.
51. **Scherer, P. E., R. Y. Lewis, D. Volonté, J. A. Engelman, F. Galbiati, J. Couet, S. Kohtz, E. van Donselaar, P. Peters, and M. P. Lisanti.** 1997. Cell-type and tissue-specific expression of caveolin-2: caveolins 1 and 2 co-localize and form stable hetero-oligomeric complexes in vivo. *J. Biol. Chem.* **272**:29337–29346.
52. **Schmid, S.** 1997. Clathrin-coated vesicle formation and protein sorting: an integrated process. *Annu. Rev. Biochem.* **66**:511–548.
53. **Schnitzer, J. E., D. P. McIntosh, A. M. Dvorak, J. Liu, and P. Oh.** 1995. Separation of caveolae from associated microdomains of GPI-anchored proteins. *Science* **269**:1435–1439.
54. **Schnitzer, J. E., P. Oh, B. S. Jacobson, and A. M. Dvorak.** 1995. Caveolae from luminal plasmalemma of rat lung endothelium: microdomains enriched in caveolin, Ca²⁺-ATPase, and inositol triphosphate receptor. *Proc. Natl. Acad. Sci. USA* **92**:1759–1763.
55. **Smart, E. J., G. A. Graf, M. A. McNiven, W. C. Sessa, J. A. Engelman, P. E. Scherer, T. Okamoto, and M. P. Lisanti.** 1999. Caveolins, liquid-ordered domains, and signal transduction. *Mol. Cell. Biol.* **19**:7289–7304.
56. **Smart, E. J., Y.-S. Ying, C. Mineo, and R. G. W. Anderson.** 1995. A detergent-free method for purifying caveolae membrane from tissue culture cells. *Proc. Natl. Acad. Sci. USA* **92**:10104–10108.
57. **Sot, J., M. I. Collado, J. L. R. Arrondo, A. Alanso, and F. M. Goui.** 2002. Triton X-100-resistant bilayers: effects of lipid composition and relevance to the raft phenomenon. *Langmuir* **18**:2828–2835.
58. **Souto, R. P., G. Vallega, J. Wharton, J. Vinten, J. Trantum-Jensen, and P. F. Pilch.** 2003. Immunopurification and characterization of rat adipocyte caveolae suggest their dissociation from insulin signaling. *J. Biol. Chem.* **278**:18321–18329.
59. **Stoorvogel, W., V. Oorschot, and H. J. Geuze.** 1996. A novel class of clathrin-coated vesicles budding from endosomes. *J. Cell Biol.* **132**:21–33.
60. **Tan-Wilson, A. L., M. Reichlin, and R. W. Noble.** 1976. Isolation and characterization of low and high affinity goat antibodies directed to single antigenic sites on human hemoglobin. *Immunochemistry* **13**:921–927.
61. **Uittenbogaard, A., Y.-S. Ying, and E. J. Smart.** 1998. Characterization of a cytosolic heat-shock protein-caveolin chaperone complex. *J. Biol. Chem.* **273**:6525–6532.
62. **Wines, B. D., and S. B. Easterbrook-Smith.** 1991. The Fab/c fragment of IgG produced by cleavage at cyanocysteine residues. *Mol. Immunol.* **28**:855–863.
63. **Xu, A., A. R. Bellamy, and J. A. Taylor.** 2000. Immobilization of the early secretory pathway by a virus glycoprotein that binds to microtubules. *EMBO J.* **19**:6465–6474.
64. **Yarbrough, T. L., T. Lu, H.-C. Lee, and E. F. Shibata.** 2002. Localization of cardiac sodium channels in caveolae-rich membrane domains: regulation of sodium current amplitude. *Circ. Res.* **90**:443–449.
65. **Zhang, M., C. Q. Y. Zeng, A. P. Morris, and M. K. Estes.** 2000. A functional NSP4 enterotoxin peptide secreted from rotavirus-infected cells. *J. Virol.* **74**:11663–11670.